ASME Journal of Turbomachinery
Online journal at:
https://asmedigitalcollection.asme.org/turbomachinery

Douglas Straub[1]
National Energy Technology Laboratory,
Morgantown, WV 26505
e-mail: douglas.straub@netl.doe.gov

Justin Weber
National Energy Technology Laboratory,
Morgantown, WV 26505
e-mail: justin.weber@netl.doe.gov

Arnab Roy
National Energy Technology Laboratory,
Morgantown, WV 26505
e-mail: arnab.roy@ge.com

Chien-Shing Lee
School of Aeronautics and Astronautics,
Purdue University,
West Layfayette, IN 47907
e-mail: cslee@purdue.edu

Tom I-P. Shih
School of Aeronautics and Astronautics,
Purdue University,
West Layfayette, IN 47907
e-mail: tomshih@purdue.edu

Effects of Downstream Vortex Generators on Film Cooling a Flat Plate Fed by Crossflow

Counter-rotating vortices, formed by the interaction of film-cooling jets and the hot gas flow, adversely affect the performance of conventional film-cooling designs. Downstream vortex generators have been shown to improve cooling effectiveness by mitigating the effects of the counter-rotating vortices and by deflecting the cooling jet laterally. In this study, computational and experimental methods were used to examine how cylindrical film-cooling holes ($D = 3.2$ mm, $L/D = 6$, $p/D = 3$, $\alpha = 30$ deg) with and without downstream vortex generators perform when the coolant supply channel is perpendicular to the direction of the hot gas. For this study, the hot gas had a temperature of 650 K and an average Mach number of 0.23. The hot-gas-to-coolant temperature ratio was 1.9, and two blowing ratios (0.75 and 1.0) were studied. Results from the computational fluid dynamics study show how crossflow affects the interaction between the film-cooling jet and hot gas flow with and without downstream vortex generators. The experimental measurements were based on infrared thermography in a conjugate heat transfer environment. Results were obtained for film-cooling performance in terms of overall effectiveness, film effectiveness, and local heat transfer coefficients. The downstream vortex generators can increase the laterally averaged effectiveness by a factor of 1.5 relative to cylindrical holes, but this higher performance is restricted to low crossflow velocities and higher blowing ratios.
[DOI: 10.1115/1.4064316]

Keywords: computational fluid dynamics (CFD), fluid dynamics and heat transfer phenomena in compressor and turbine components of gas turbine engines, heat transfer and film cooling, measurement techniques

Introduction

Advanced gas turbines use film cooling to protect components in the hot gas path. Although significant progress has been made over the last 50 years [1–4], advanced cooling technologies can still impact cycle performance. For example, a recent sensitivity study on natural gas combined cycles suggests that a 44% improvement in film-cooling effectiveness translates to a 2.5 percentage point improvement (or 4% change) in the combined cycle efficiency relative to a 62% baseline [5].

Film cooling protects hot gas components in a gas turbine engine by forming an insulating layer of cooler air to isolate the surface from the hot gases [6]. With discrete cooling jets formed by inclined circular holes, the interactions between the cooling flow and the hot gases create a pair of counter-rotating vortices (CRVs) [7,8]. These CRVs can cause the cooling jet to lift from the surface, and the insulating layer of cooling air is subsequently replaced with hot gas infiltration near the surface. Thus, CRVs can significantly diminish the effectiveness of film cooling.

Several prior efforts have been proposed to mitigate the impact of CRVs on film-cooling performance. These prior methods have been classified into four categories by Lee et al. [9]:

- Modify the shape and/or orientation of the film-cooling holes. For example, shaped holes [10–14], compound-angle holes [15–20], and slots have been used to reduce the negative effects of CRVs.
- Change the layout of the film-cooling arrays such that the CRVs entrain cooler air instead of hot gases. For example, two rows of film-cooling holes arranged in a staggered fashion provide cooler air to the downstream region between the cooling jets.
- Incorporate modifications to mitigate CRV formation mechanisms and/or minimize the strength of CRVs. For example, transverse surface trenches [21] and upstream ramps [22] have been studied as an approach to reduce the effects of CRVs.
- Create vortical structures that have an opposite direction (i.e., anti-CRVs) to counteract conventional CRV degradation. Some examples include struts [23], upstream and downstream tabs [24,25], side jets to create anti-kidney vortices [26], and vortex generators. [27–31].

Background: Vortex Generators for Film Cooling. This study focuses on the use of vortex generators to create vortical structures

[1]Corresponding author.

Contributed by the International Gas Turbine Institute (IGTI) of ASME for publication in the Journal of Turbomachinery. Manuscript received September 13, 2023; final manuscript received November 20, 2023; published online xx xx, xxxx. Tech. Editor: David G. Bogard.

with a different directional sense relative to conventional CRVs. The use of vortex generators (VGs) was first proposed by Rigby and Heidman in 2008 [27]. A V-shaped tetrahedron with an isosceles triangle at the base and an apex that is perpendicular to that triangle was used as a VG. This VG, henceforth denoted as a delta ramp, is placed downstream of the film-cooling hole with the apex of the V-shaped tetrahedron facing the film-cooling hole. Q6 Using RANS simulations, the delta ramp generates a pair of anti-CRVs that entrains the film-cooling flow back to the surface to increase the lateral spreading of the coolant film and counteract the CRV performance degradation effects. In a later study, Zaman et al. [28] experimentally concluded the following: (1) the best height for the delta ramp is 0.75D, where D is the diameter of the film-cooling hole; (2) sharp edges are better than having rounded ones; and (3) the delta ramp should be placed 1D–3D downstream of the film-cooling hole. Song et al. [29] conducted an experimental study on the effects of the inclination angle of the delta ramp. For a range of blowing ratios, the best film effectiveness was observed with a delta ramp inclination of 20 deg.

Lee et al. [9] proposed a different type of VG, and this prior work was the basis for the VG design considered in this paper. Instead of a single delta ramp, a pair of rectangular plates arranged in a V-shape is placed at a distance 1D downstream of the film-cooling hole (see Fig. 1). The height of the VGs studied in this paper is 0.5D. Based on prior work, the film-cooling effectiveness is improved by two mechanisms. First, the two rectangular plates act as guide vanes that divert the cooling flow laterally. The delta ramp generates a similar flow feature, but the diversion is due to blockage instead of guide vanes. Most of the diverted flow from the inclined portion of the delta ramp forms anti-CRVs. Second, instead of shedding vortices like in the delta ramp, the leading edges of the V-shaped VGs induce the formation of horseshoe vortices with a direction (sense) that is opposite of the traditional CRV. Along the downstream face of the V-shaped VGs, the vortices near the surface entrain the cooler flow back to the surface. This reduces jet lift-off and increases lateral film coverage as described in Lee et al. [9]. Based on these previous RANS studies, VGs with this functional design could increase film-cooling effectiveness by 50–100% and outperform fan-shaped holes, W-shaped holes, flow-aligned blockers, and upstream ramps.

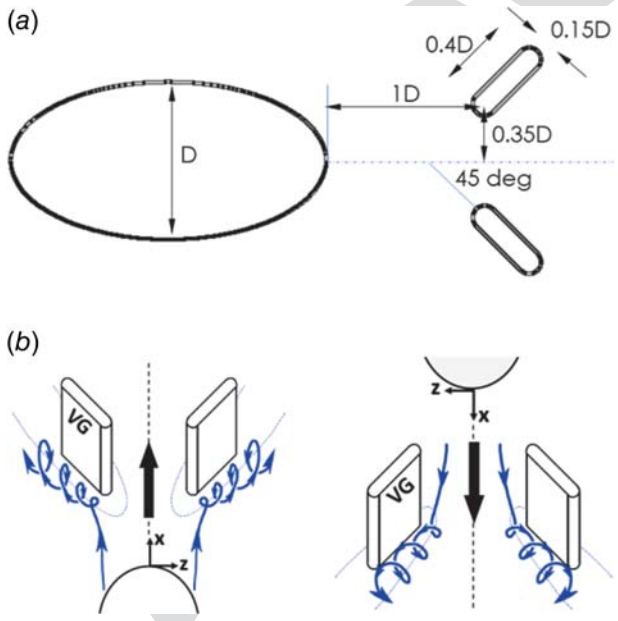

Fig. 1 V-shaped downstream vortex generators (DVGs): (*a*) plan view and (*b*) schematic of horseshoe vortices formation along the pressure and suction side of the DVGs (adapted from Lee et al. [30]).

This paper is an extension of previous efforts by Lee et al. [9,30]. Although this paper contains both numerical and experimental results, the primary focus is the experimental verification in a conjugate heat transfer test rig. In addition, this paper compares the present results in a crossflow coolant channel configuration, whereas the previous efforts only considered plenum-fed coolant supply configurations.

Background: Film-Cooling Effectiveness (Adiabatic and Conjugate). As described by Goldstein [6], the film temperature can be used as a representative reference temperature to estimate the heat flux between the hot gas and a film-cooled surface. Figure 2 depicts an analogous thermal resistance network without a thermal barrier coating. The important quantities from Fig. 2 that will be discussed include the film effectiveness, η_f, the film temperature, T_f, and the external heat transfer coefficient due to film cooling, h_f. Although the film effectiveness, η_f, depends on numerous factors, it is typically defined (see Eq. (1)) as the ratio of the actual reduction in driving temperature ($T_g - T_f$) relative to theoretical maximum temperature difference ($T_g - T_{c,e}$). As described by Bunker [4], adiabatic wall experiments provide an ideal and limiting case for laboratory studies, but the application of film cooling in a real engine does not involve an adiabatic boundary. The term "adiabatic film effectiveness" may be confusing in the context of a conjugate heat transfer environment, so for the remainder of this paper, the term "film effectiveness" will be used instead of "adiabatic film effectiveness." This paper will show how the film effectiveness varies for film-cooling holes with and without downstream vortex generators with a coolant supply channel that is perpendicular to the hot gas path.

The film temperature can be defined in terms of the film effectiveness, η_f (see Eq. (2)). For the case of no film cooling ($\eta_f = 0$), the film temperature is equal to T_g, the freestream gas temperature. When film cooling is present, the film temperature is a mixture of $T_{c,e}$ and T_g. The film temperature also has a strong spatial variation depending on the location relative to the cooling hole exit.

If film-cooling experiments are conducted under adiabatic conditions (i.e., $k_w = 0$), then the local wall temperature is the same as the local film temperature (see Eq. (3)). According to Bohn et al. [31], the energy exchange between the fluid and the wall can alter the secondary flows near the surface. These secondary flow structures can play an important role in the local film temperature and film effectiveness. Ramachandran and Shih [32] have also shown the importance of thermal conductivity (Biot Number) for scaling heat flux and temperature distributions. The computational portion of this paper will consider both adiabatic and conjugate boundary conditions along a flat plate.

Figure 2 also shows that the external heat transfer coefficient changes when film coolant is present. The interactions between the film-cooling jets and the hot gas can increase the local heat transfer coefficients, so potential benefits in film effectiveness can be offset by heat transfer augmentation. In this paper, experimental measurements of both the local film effectiveness and the local heat transfer coefficients will be discussed.

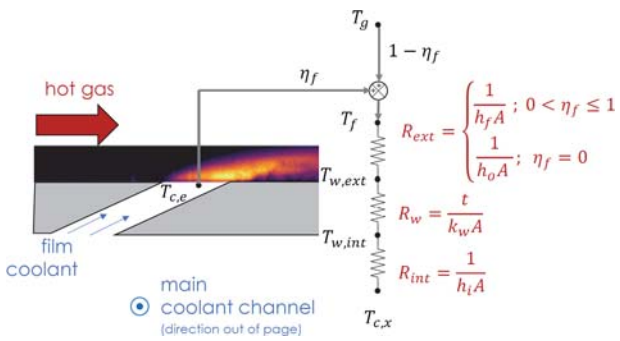

Fig. 2 Schematic of film-cooling thermal resistance network

$$\eta_f = \frac{T_g - T_f}{T_g - T_{c,e}} \tag{1}$$

$$T_f = \eta_f T_{c,e} + (1 - \eta_f) T_g \tag{2}$$

$$q''_f = h_f (T_f - T_w) \tag{3}$$

Background: Film Cooling—Effects of Coolant Crossflow. Numerous studies have considered the effects of a crossflow coolant configuration. In 1997, Thole et al. [33] showed that the downstream cooling film is affected by the cooling hole inlet conditions and local separation bubbles inside the cooling holes. Kohli and Thole [34] showed that perpendicular crossflow configurations had a major effect on film effectiveness and discharge coefficients. On the other hand, Kohli and Thole [34] showed that co-flow and counter-flow configurations were very similar to a plenum-fed configuration. In subsequent years, several studies have shown that crossflow degrades the film cooling and discharge coefficient performance for shaped holes [35–40]. Gritsch et al. [41] have shown that the film effectiveness in the near-hole region could be altered by over 100% for the perpendicular crossflow conditions. In addition to the significant degradation for shaped film-cooling holes, Gritsch et al. [41] also reported a mild improvement in film effectiveness for cylindrical holes. Stratton [42] and Qenawy et al. [43] show how the perpendicular crossflow generates secondary flow structures inside the cooling hole that subsequently impact the downstream cooling jet structure. More recently, Sperling and Mathison [44] reported that the coolant swirl and flow biasing within the film-cooling jet could be less susceptible to freestream turbulence and temporal fluctuations.

Although the prior work considered either cylindrical and/or shaped film-cooling holes, there are two relevant publications on downstream vortex generators with perpendicular crossflow. In 2017, Song et al. [29] used particle imaging velocimetry to show how a triangular pyramid vortex generator located immediately downstream of the film-cooling hole produced an "anti-counter-rotating vortex pair" to prevent lift-off and increase coolant jet spreading near the surface. For a blowing ratio (BR) of 1.0, Song et al. [29] reported that these downstream vortex generators (DVGs) increased the area-averaged film-cooling effectiveness from about 0.1 for a cylindrical hole to about 0.2 when a vortex generator was located downstream of the hole. In 2022, Wang et al. [45] also studied a perpendicular crossflow coolant configuration for cylindrical and shaped holes with and without DVGs. Wang et al. [45] reported that the film effectiveness for the cylindrical hole increased from about 0.1 (no DVGs) to about 0.15 with DVGs. Therefore, these prior studies using a different DVG design have shown a film effectiveness improvement that is 1.5–2.0 times higher than a baseline cylindrical hole. Neither the local heat transfer coefficients nor the overall cooling effectiveness have been reported in this prior work.

The DVG design discussed in this paper is shown in Fig. 1 and differs from Song et al. [29] and Wang et al. [45]. This DVG design was developed by Lee et al. [9,30] using a cooling supply plenum configuration. The current paper will investigate the performance of a DVG design that is identical to Lee et al. [30] except for a perpendicular coolant crossflow configuration. In addition, local heat transfer coefficients, film effectiveness, and overall cooling effectiveness will be experimentally measured using a conjugate heat transfer test facility.

Motivation and Objective. If the film-cooling effectiveness (and internal cooling efficiency) can be improved, Uysal [5] has shown large benefits in efficiency, greenhouse gas emissions, and power for combined cycle systems. The objective of this effort is to investigate whether a relatively new idea for DVGs is a feasible approach to achieve higher film-cooling effectiveness in a perpendicular crossflow configuration.

Computational Setup

The computational study described in this section seeks to provide some qualitative understanding of the film-cooling jet formation within the film-cooling hole and the subsequent interactions with the mainstream as the coolant channel velocity is increased. These computational fluid dynamics (CFD) results explain some unexpected experimental results and guide the data analysis reported in this paper.

Description of the Computational Fluid Dynamics Problem. Figure 3 shows a schematic of the film-cooling configuration

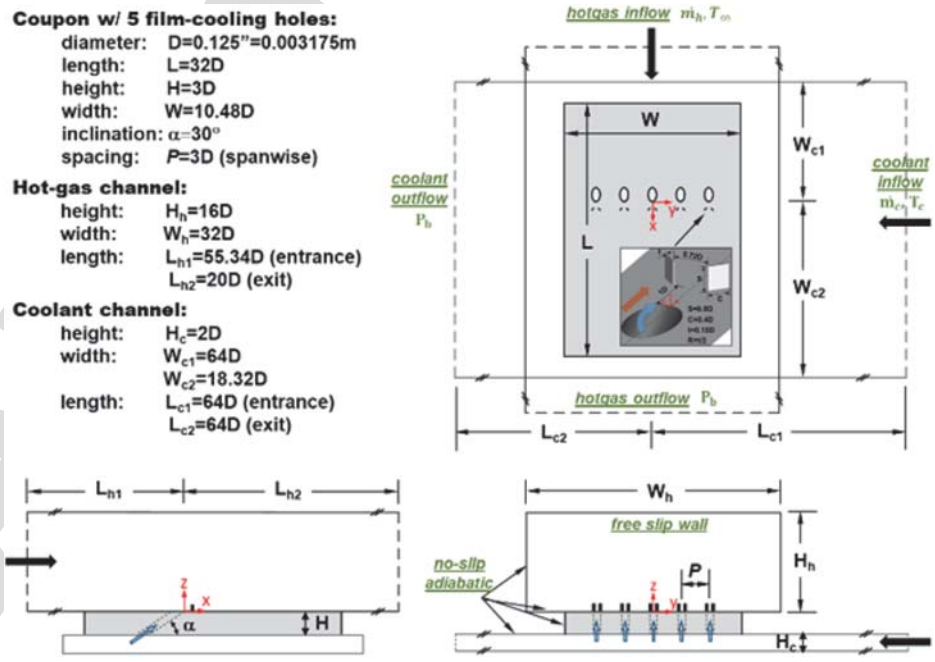

Fig. 3 Schematic of the computational problem studied

Table 1 Summary of all CFD cases studied

Case	BR	Coolant channel velocity, V_{ch}	Thermal BC on coupon	DVGs applied
1	0.75	20 m/s	Adiabatic	No
2				Yes
3			Conjugate	No
4				Yes
5		40 m/s	Adiabatic	No
6				Yes
7			Conjugate	No
8				Yes
9	1.0	20 m/s	Adiabatic	No
10				Yes
11			Conjugate	No
12				Yes
13		40 m/s	Adiabatic	No
14				Yes
15			Conjugate	No
16				Yes

studied computationally and experimentally. All dimensions are given in terms of the film-cooling hole diameter, $D = 3.175$ mm. The geometry for the CFD is identical to the experimental facility except for the distance from the inflow boundary on the hot gas side, L_{h1}. L_{h1} was chosen to ensure that the CFD velocity profiles match the previously published experimental velocity profiles [30]. The geometry of the downstream vortex generators is shown in Fig. 1.

The hot gas has a freestream temperature of $T_g = 650$ K and a freestream velocity of $V_g = 107.5$ m/s along the x-direction. The flow in the boundary layer is assumed to be turbulent from the leading edge of the flat plate. The coolant channel conditions include an inlet temperature, $T_{c,I}$, of 345 K, which targets a density ratio of DR = 1.9. Two different "mean" coolant channel velocities, V_{ch}, of 20 and 40 m/s and two blowing ratios of BR = 0.75 and 1.0 are studied for comparison. A summary of all simulations performed is given in Table 1.

Formulation, Numerical Method of Solution, and Code. In this study, the governing equations employed for the gas phase are the ensemble-averaged continuity, Navier–Stokes, and energy equations (often referred to as RANS) for a thermally perfect gas with temperature-dependent thermal conductivity, viscosity, and specific heat for air. The effect of turbulence is modeled using the SST model with curvature correction and production limiter [46]. Though RANS models are known to underpredict lateral spreading of film-cooling flows, Lee et al. [30] have shown that once vortex generators are added downstream of the film-cooling hole, the SST model provides excellent results. In that paper, the SST model was validated by comparing the measured velocity profiles upstream and downstream of the film-cooling hole, as well as the wall temperatures.

In the current study, the film-cooling holes are fed in a crossflow fashion, which produces a swirl in each film-cooling hole. For such flows, Stratton et al. [42] showed the large eddy simulation solution was between the k-ϵ and SST predictions. In this study, the SST model was chosen because the solutions generated in this study will be compared with those of Lee et al. [30], which also used the SST model.

For the conjugate simulations, the temperature-dependent thermal conductivity given in Ref. [47] is used. The solid phase is coupled to the gas by requiring the temperature and the heat flux at the gas–solid interfaces to be the same. Solutions to the governing equations were obtained using ANSYS FLUENT [48]. Since only steady-state solutions were sought, the SIMPLE algorithm was used. The fluxes for density, momentum, and energy at the cell faces were interpolated by using the second-order upwind scheme. Pressure and all diffusion terms were approximated by using second-order accurate central formulas. For the solid phase, there are only diffusion terms, and they were approximated by using second-order accurate central formulas. For all computations, iterations were continued until all residuals for all equations plateaued to steady-state. At convergence, the scaled residuals were less than 10^{-5} for continuity and momentum, less than 10^{-7} for energy, and less than 10^{-5} for the turbulence quantities.

Verification and Validation. Verification was accomplished via a grid-sensitivity study. Figure 4 shows the multi-block structured grid system used, where grid points were clustered to all solid surfaces, smooth, and nearly orthogonal. The following three grid sizes were examined: mesh 1, the coarsest grid, had

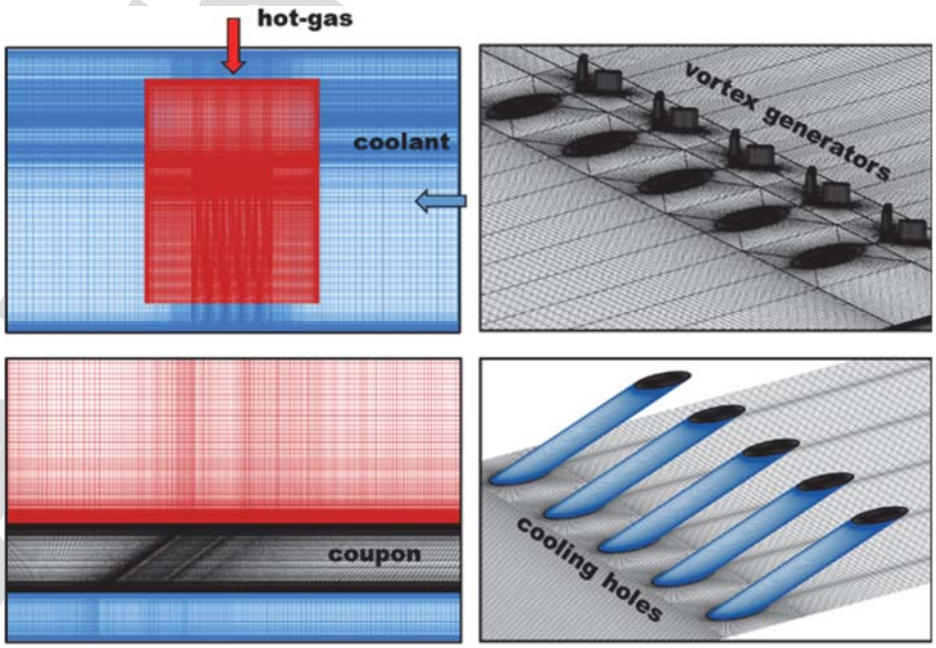

Fig. 4 Grid system used in the CFD model

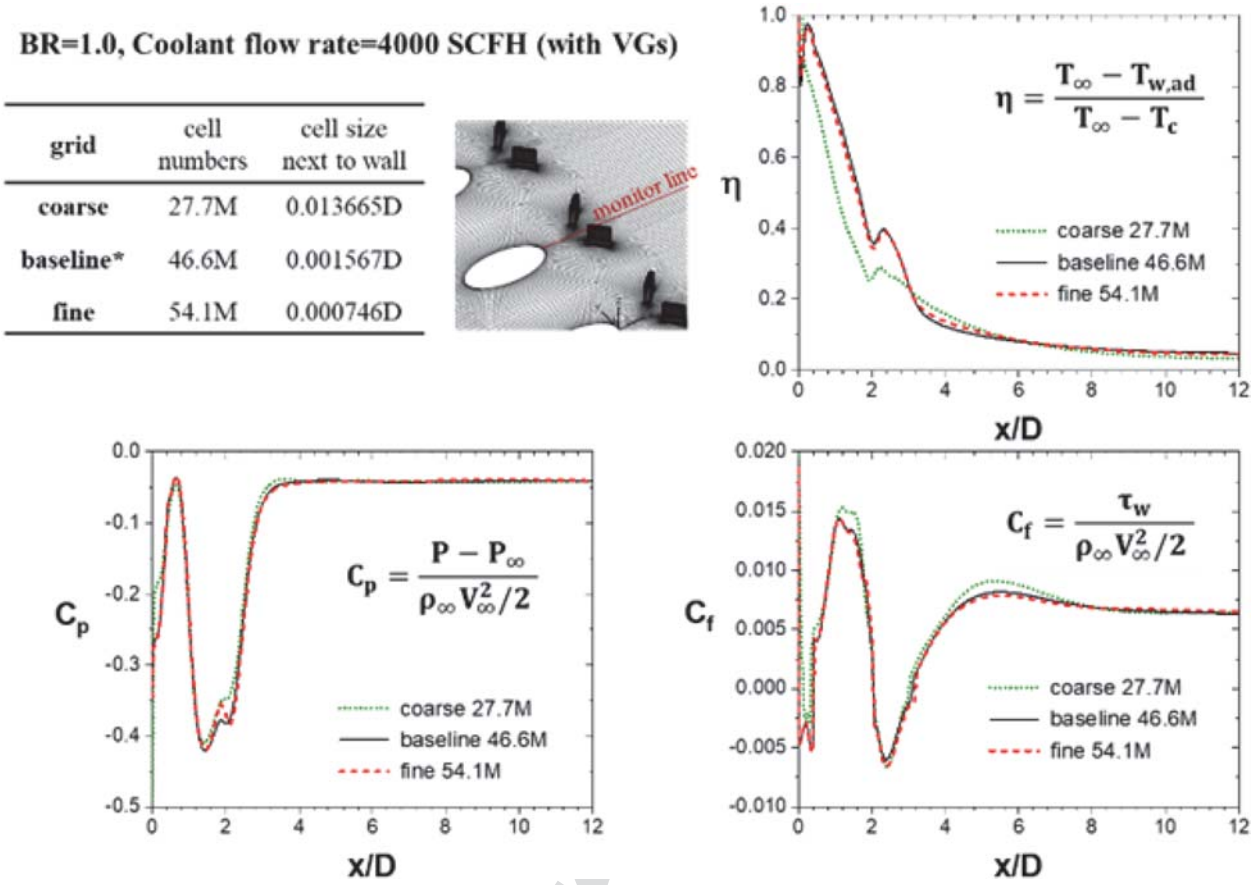

Fig. 5 Grid sensitivity: C_p, C_f, and η along x at $y = z = 0$

27.7 million cells; mesh 2, the baseline grid, had 46.6 million cells; and mesh #3, the finest grid, had 54.1 million cells. Note that mesh 3 refined mesh 2 only in the regions where hot gas and the cooling flow interact.

For all three grids, the first cell away from all solid surfaces has a $y+$ less than unity. The grid-sensitivity study is performed using parameters in case 14 (see Table 1). Figure 5 shows the pressure coefficient (C_p), the skin friction coefficient (C_f), and the centerline film-cooling effectiveness (η) for all three mesh resolutions. In this figure, the solutions of C_p, C_f, and η nearly coincide as the grid is refined, except for a small difference in C_p around $x/D = 2$ where flow separation occurs. Based on this study, the baseline grid (see Fig. 5) was used to generate all subsequent solutions.

Experimental Setup

The objective of the experimental effort is to evaluate the film-cooling performance of the V-shaped DVGs developed by Lee et al. [9,30] under conditions of perpendicular coolant crossflow. Although the performance of this DVG design is encouraging for a plenum configuration [30], the effects of perpendicular coolant crossflow were not understood prior to this work. This paper will discuss spatially resolved heat transfer coefficients, film effectiveness, and average overall cooling effectiveness for a single row of cylindrical film holes with and without DVGs.

Experimental Formulation and Approach. The experimental approach is similar to Gritsch et al. [37] and Kneer et al. [49], but the governing equation has been modified to eliminate the film temperature from the regression model (see Eq. (4)). In prior work [37,49], water-cooling channels were used to control the wall temperature. The heat flux at the surface was found using a finite element model. Equation (3) was used as the basis for a linear regression model in which the heat transfer coefficient is simply the slope of the regression equation. When the regression is performed at each pixel in an infrared thermal image, local heat transfer coefficients can be calculated for a set of experimental wall temperatures.

The approach taken in this paper combines Eqs. (2) and (3) to eliminate the film temperature, as shown in Eq. (4). The gas temperature, T_g, and the coolant inlet temperature, $T_{c,i}$, are kept constant at 650 K and 345 K, respectively. Infrared temperature measurements from both the hot and cold sides of the flat plate are used as boundary conditions in a commercial three-dimensional finite element solver (ANSYS-Mechanical 2022 R1). The finite element model calculates the heat flux distribution for the region of interest on the flat plate. In this effort, the local surface heat flux, q_f'', and the local surface temperature, T_w, are varied by changing the heat transfer coefficient on the cold side of the plate. Using data from the different heat flux conditions, the local heat transfer coefficient, h_f, and film effectiveness, η_f, were found from a linear regression analysis performed at each pixel.

$$\frac{q_f''}{T_g - T_{c,e}} = h_f\left(\frac{T_g - T_w}{T_g - T_{c,e}}\right) - h_f\eta_f \tag{4}$$

This approach is based on two key assumptions. First, the external thermal resistance and the film temperature must be independent of variations in the internal cooling channel velocity (i.e., the variable used to change the heat flux in this study). The limits of this assumption will be discussed in greater detail in subsequent sections. Second, the coolant exit temperature, $T_{c,e}$, is assumed to be equal to the coolant inlet temperature, $T_{c,i}$. This assumption implies that no heat is transferred to the coolant within the coolant holes. To minimize heat transfer to the coolant inside the

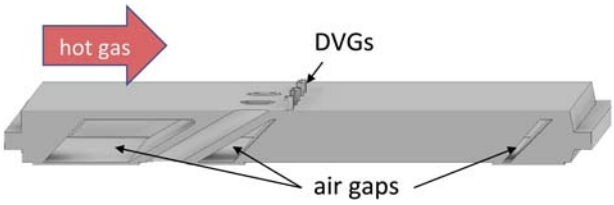

Fig. 6 Cross-section of film-cooled test article

cooling holes, the cooling holes are thermally isolated using air gaps for 80–85% of the plate thickness (see Fig. 6).

A sequential perturbation analysis was completed to estimate the error associated with this approach. From this analysis, the errors in the heat transfer coefficient were less than 10%. However, the standard errors of the slope (heat transfer coefficient) were on the order of +15–20%, and the standard error of the intercept was +20–30% for the film effectiveness.

Test Facility. The test facility used in this effort has been described previously by Ramesh et al. [50], so only the key features will be described in this section. For the purposes of this paper, the temperature ratio, $T_g/T_{c,i}$, has been held constant at a value of 1.88 to be consistent with prior work [30]. The hot gas temperature is kept constant at 650 K, and a 3.2-mm-diameter type-K thermocouple measures the gas temperature upstream of the film-cooling test article. More details of the inlet temperature and velocity profiles have been published previously [30]. The hot gas mass flow is kept constant using a high-temperature flow control valve and an orifice flowmeter. A flow conditioning section produces a uniform flow entering a convergent nozzle at the inlet to the 101 × 101-mm test section. The test section is designed with three viewports that can be used for laser diagnostics and infrared imaging (see Fig. 7). For the results discussed in this paper, sapphire windows were used to measure infrared emission from the hot and the cold surfaces. Stainless steel blanks were installed in the viewport walls adjacent to the test article.

The coolant channel is a 127 × 6.4-mm rectangular channel. The coolant temperature is measured upstream and downstream using 1.6-mm-diameter type-T thermocouples. These thermocouples are located about 25 mm from the leading and trailing edges of the test coupon. An electric preheater is used to control the temperature of the cooling air. The average temperature is used as a control point to maintain a constant coolant temperature near the center hole. Since the coolant flow direction is normal to the hot gas flow direction, the flat plate test article is located at the intersection between the coolant channel and the hot gas flow channel. The cooling air flowrate is measured upstream of the film-cooling holes using a

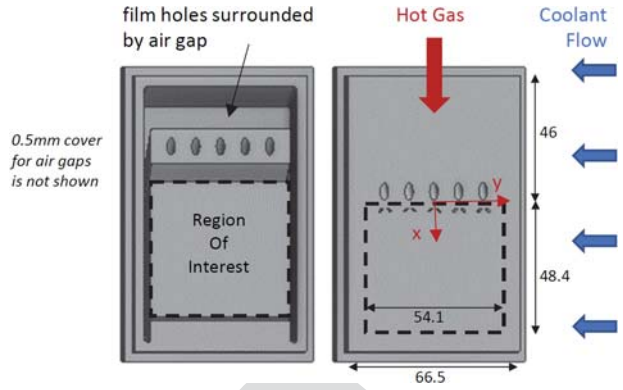

Fig. 8 Schematic of flat plate test article: origin of coordinate system and region of interest

Coriolis flowmeter (accuracy ±0.25% of reading) and downstream of the test article using an Imperial V-20THD venturi meter (accuracy ±0.75%). The film-cooling air flowrate is calculated as the difference between the cooling airflow measured upstream and downstream of the test coupon. The resulting uncertainty in the blowing ratio is +0.075 for the results presented in this paper.

A back pressure control valve is used to independently control the film-cooling airflow. The independent variables for these experiments are the cooling channel flow at the inlet to the cooling channel and the blowing ratio.

Film-Cooling Geometry. The flat plate test coupons are clamped between the external wall of the hot channel and the external wall of the coolant channel. These stainless steel coupons were additively manufactured and painted with four coats of Krylon High Heat Max paint to increase the surface emissivity. The hot surface of the test coupon is 101 mm × 66 mm, and the long side is oriented parallel to the hot gas path, as shown in Fig. 8. A 3-mm-wide sealing face (3 mm thick) encompasses the test article, and the overall thickness of the test article is 9.5 mm.

The film-cooling holes are thermally isolated for 80–85% of the test article thickness. Figure 8 also shows air gaps surrounding all four sides of the region of interest. These gaps also extend through 80–85% of the test article thickness, and the surfaces adjacent to stagnant air gaps are treated as adiabatic surfaces in the finite element model. A 0.5-mm stainless steel sheet (not shown in Fig. 8 for clarity) is spot welded to the cold side to approximate a flush surface with the interior wall of the coolant channel while maintaining the insulating air gaps.

The cylindrical film-cooling holes have a diameter $D = 3.2$ mm, and the center hole is located along the mid-plane of the test

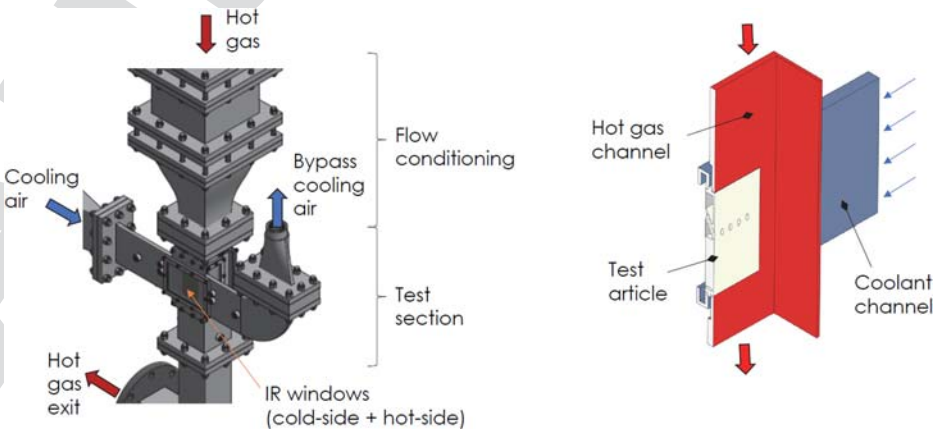

Fig. 7 Schematic of test facility (insulation is not shown in this figure)

Table 2 Film-cooling hole design and experimental constants

Parameter	Design value
Cooling hole diameter, D	3.2 mm
Cooling hole pitch (p/D)	3
Cooling hole length (L/D)	6
Number of cooling holes	5
Mainstream gas temperature	650 K
Mainstream velocity, V_g	110 m/s
Mach number—hot gas	0.22
Reynold's number based on hole diameter ($\rho_g V_g D/\mu_g$)	6180
Mainstream turbulent intensity	<2%
Approach boundary layer thickness (δ/D)	1.1 (at LE of film hole) 0.99 ($x=-10D$)
Temperature ratio (T_g/T_c)	1.88
Coolant channel hydraulic diameter, D_h	12.1 mm

coupon (a total of five cooling holes). Table 2 summarizes the cooling hole design. The downstream vortex generators are rectangular prisms oriented in a V-shape with a width of $0.4D$, a height of $0.5D$, and a thickness of $0.15D$. See Fig. 1 for more details on the vortex generator design.

The surface roughness for the DVG test article was measured before and after painting. The centerline average roughness height (Ra) was approximately 5 μm before painting and about 2.5 μm after painting. As described by Bons [51], there are numerous correlations to relate Ra to an equivalent sand grain roughness, k_s. In a previous study by Searle et al. [52], the Schaffler [53] correlation ($k_s = 8.9$ Ra) matched measured friction factors reasonably well for additively manufactured surface roughness. To estimate the roughness flow regime for the current work, the non-dimensional roughness parameter, $k^+ = \rho_w k_s u_\tau/\mu_w$, has been evaluated. Based on the CFD results, the shear velocity upstream of the film-cooling holes is about 5.3 m/s, so $k+<5$. From a surface roughness perspective, the flow can be considered hydrodynamically smooth.

Infrared Thermal Imaging. The dependent variables from this experiment include the surface temperature distributions for both the hot and cold sides of the test coupon. Two identical infrared cameras (FLIR Model A8300sc) are used to measure these surface temperatures. The cameras are calibrated against a blackbody source (Infrared Systems IR-564/301) prior to testing. In addition, "in situ" calibrations are used to characterize background radiation, window transmissivity, internal reflections, and other factors, as described by Ramesh et al. [50]. The root-mean-square error between the infrared and the in situ calibration temperature measurements is less than 3 K.

Table 3 Experimental test plan—independent variables

Parameter	Design value
Blowing ratio ($\rho_c V_j/\rho_g V_g$)	BR = 0.75 & BR = 1.00
Nominal coolant channel velocity, $V_{ch,i}$	10, 15, 20, 30, 40 m/s
Density ratio (ρ_c/ρ_g)	1.91–1.94 (BR = 0.75) 1.94–1.99 (BR = 1.00)
Reynold's number—coolant channel hydraulic diameter ($Re_{D_h} = \rho_c V_{ch,i} D_h/\mu$)	7300–29,300
Mach number—coolant channel	<0.12
VR_i ($V_{ch,i}/V_j$)	0.25–1.03 (BR = 0.75) 0.19–0.77 (BR = 1.0)
VR_{ch} ($V_{ch,i}/V_g$)	0.1–0.4
Film mass fraction ($\dot{m}_f/\dot{m}_{ch}$)	19–4% (BR = 0.75) 25–6% (BR = 1.00)

Test Conditions. The test facility conditions that are kept constant are summarized in Table 2. The independent variables are summarized in Table 3. By varying the coolant channel velocity, the heat transfer coefficient on the cold side of the test coupon changes, and that, in effect, changes the wall temperature on the hot side. Data collection is performed after the steady-state condition is reached, and the process data are averaged over a ten-minute window. Each test condition is replicated.

Results and Discussion

Wall Temperature Contours. For BR = 1.0, the hot-side surface temperature measurements are shown in Fig. 9. The hot gas flow direction is from left to right, and the coolant flow direction is from top to bottom. The channel velocity was varied to produce a range of coolant hole inlet velocity ratio conditions ($0.19 \le V_{ch,i}/V_j \le 0.77$). The advantage of the DVGs is clearly seen at the lowest crossflow channel velocity (Fig. 9, top row). However, as the crossflow channel velocity increases, the DVG performance seems to degrade, and cylindrical holes without DVGs perform better at the highest crossflow channel velocity (Fig. 9, bottom row).

This degradation in cooling performance can also be observed if the wall temperature is averaged over the region of interest and plotted as a function of the hole inlet velocity ratio, as shown in Fig. 10. At a blowing ratio of 0.75, the DVGs provide no significant benefit (i.e., the average wall temperatures in the region of interest are higher than the cylindrical holes). At a blowing ratio of 1.0, the DVGs provide a benefit if the coolant channel velocity is less than 50–60% of the calculated mean cooling hole velocity. However, the cooling effectiveness of the DVGs changes abruptly for an inlet hole velocity ratio greater than 0.5.

Similar abrupt changes have been observed previously. For a 777-shaped cooling hole under perpendicular crossflow, Qenary et al. [43] reported that the area-averaged effectiveness suddenly increased for hole inlet velocity ratios of approximately 0.5, but the impact on wall temperature was not reported. Although the results of this study involve a different film-cooling hole than Qenary et al., the transition in average wall temperature observed for BR = 1.0 occurs at nearly the same hole inlet velocity ratio (i.e., 0.5). However, instead of an improvement, a degradation in cooling performance is observed in the present work.

To gain more understanding of these cooling performance curves, two blowing ratio conditions and two channel velocities were selected for a CFD study. The CFD results provide a qualitative understanding of the flow behavior inside the cooling hole.

Nature of Cooling Jet Flow From Computational Fluid Dynamics. CFD simulations were performed to investigate the measured hot-side surface temperatures, specifically the change in slope for the DVGs at BR = 1.0 (Fig. 10(*b*)). Test conditions for the CFD were chosen on both sides of this experimentally measured inflection point.

Figure 11 shows streamlines, velocity vectors, and temperature contours within (and downstream of) the film-cooling hole. The swirling flow created by the crossflow is apparent inside the film-cooling hole. For the low coolant channel velocity condition and BR = 1, the swirl momentum relative to the axial momentum of the film-cooling jet is small. The CFD results show the flow through the film-cooling holes is more uniform, like a quiescent plenum. This operating condition correlates with the conditions on the low-velocity ratio side of the inflection point in Fig. 10(*b*) (i.e., the DVG cooling performance was better than the baseline in regard to the average wall temperature in the region of interest).

For channel velocity of 20 m/s and BR = 0.75 ($VR_i = 0.51$), the relative swirl momentum is larger, and the CFD results show the

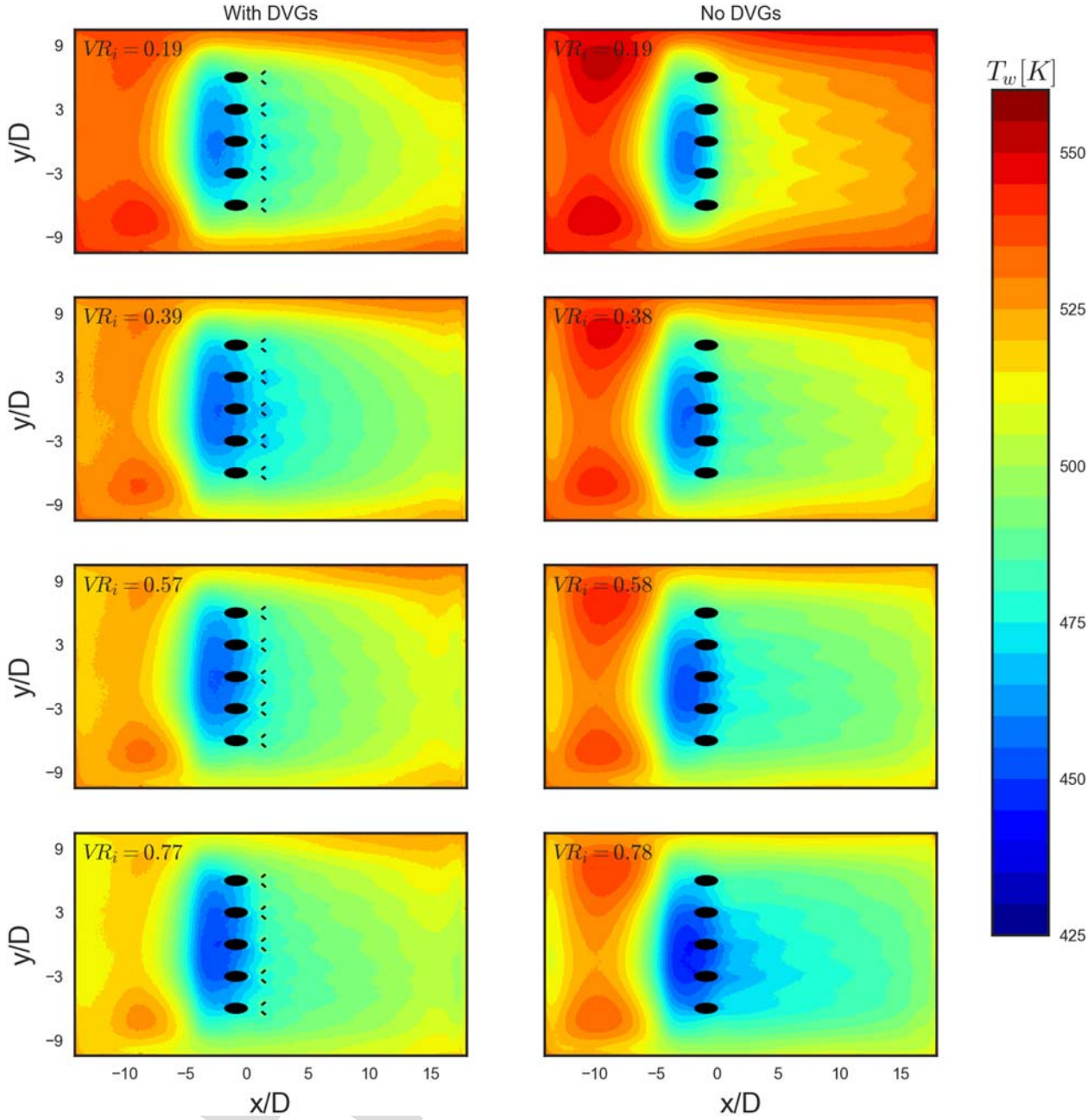

Fig. 9 Measured hot-side surface temperatures with DVGs (left) and without DVGs (right) for range of inlet hole velocity ratio conditions ($VR_i = V_{ch,i}/V_j$) and BR = 1.0

cooling jet only interacts with one of the DVGs (see Fig. 11, upper-left). This qualitative feature of the CFD flow is consistent with the experimental results (see Fig. 10(*a*)), which indicate the DVGs provide no significant benefit in regard to the average wall temperature in the region of interest.

At the higher coolant channel velocities, the swirl momentum relative to the axial film-cooling jet is stronger. The CFD results predict "lift-off" near the hole exit and entrainment of hot gas under the cooling jet. At these higher hole inlet velocity ratio conditions ($VR_i > 0.5$), the cooling jet only reacts with one of the DVGs, and jet lift-off is predicted regardless of the BR.

Based on these results, the perpendicular coolant crossflow can cause "lift-off" at lower blowing ratio conditions than typically cited for quiescent cooling plenum configurations. The momentum of the cooling jet exiting the film-cooling hole is comprised of streamwise and swirl components generated from the coolant crossflow velocity. The swirl momentum can significantly impact the nature of the film-cooling flow and the film-cooling performance. If "lift-off" occurs, only the fraction of the film-cooling jet intercepted by the DVG can be redirected. In fact, once the cooling jet "lift-off" occurs, only the leeward side of the vortex–generator pair can affect the lateral spreading of the film-cooling jet. The benefit of the DVGs diminishes when the cooling jet does not interact with both DVGs.

Overall Cooling Effectiveness. The overall cooling effectiveness is a non-dimensional wall temperature as defined in Eq. (5), so the average wall temperatures shown in Fig. 10 can be compared on a non-dimensional basis (see Fig. 12). Overall cooling effectiveness curves have not been reported previously for a perpendicular coolant crossflow configuration.

$$\phi = \frac{T_g - T_{w,ext}}{T_g - T_{c,i}} \tag{5}$$

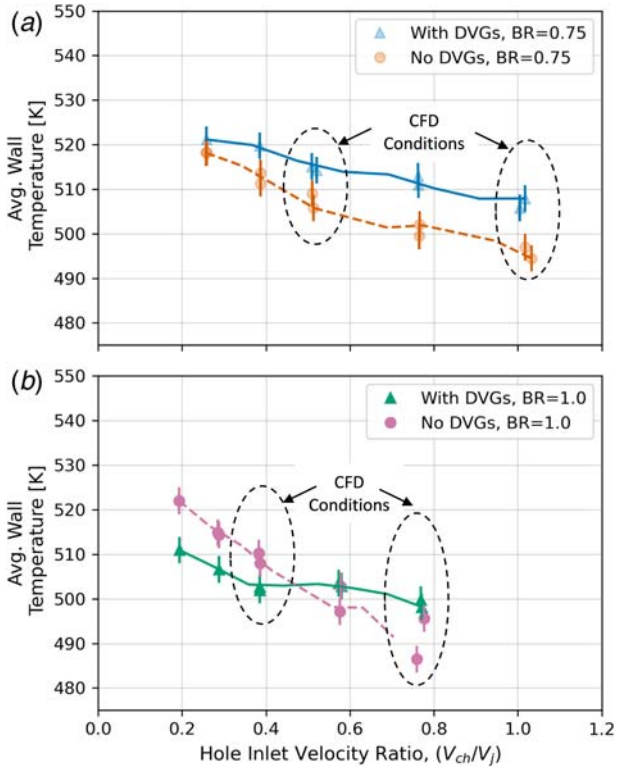

Fig. 10 Experimental area-averaged hot-side wall temperatures (+3 K) over region of interest: (*a*) BR = 0.75 and (*b*) BR = 1.0

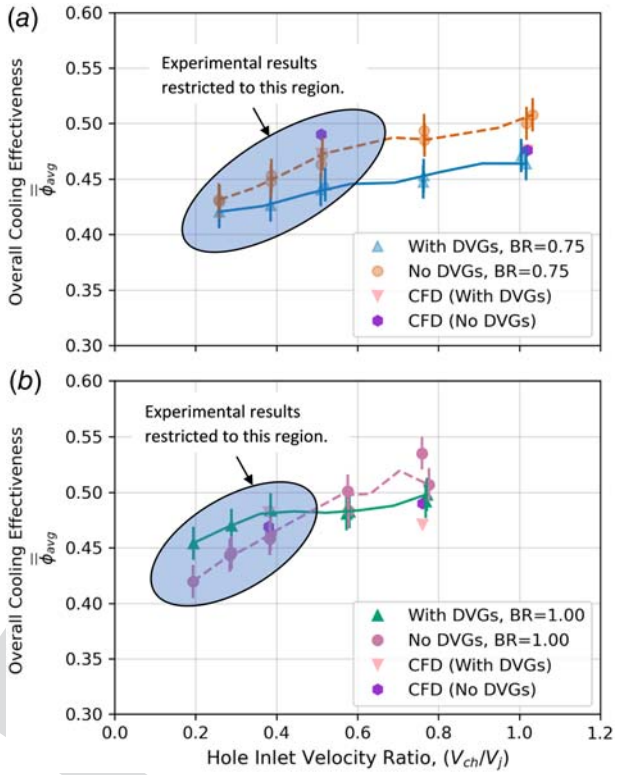

Fig. 12 Comparison of overall cooling effectiveness (+0.015) with and without DVGs: (*a*) BR = 0.75 and (*b*) BR = 1.0

As described in Table 1, both conjugate and adiabatic CFD simulations have been performed. The conjugate CFD predictions for the average cooling effectiveness are also shown in Fig. 13. For the low crossflow velocity and BR = 0.75, the cooling effectiveness is slightly better (0.49 vs 0.47) with no DVGs. At a BR = 0.75 and higher crossflow velocities, the CFD predicts a cooling effectiveness that is about the same for both configurations (i.e., 0.476). In summary, for BR = 1.0, the trend in overall effectiveness is

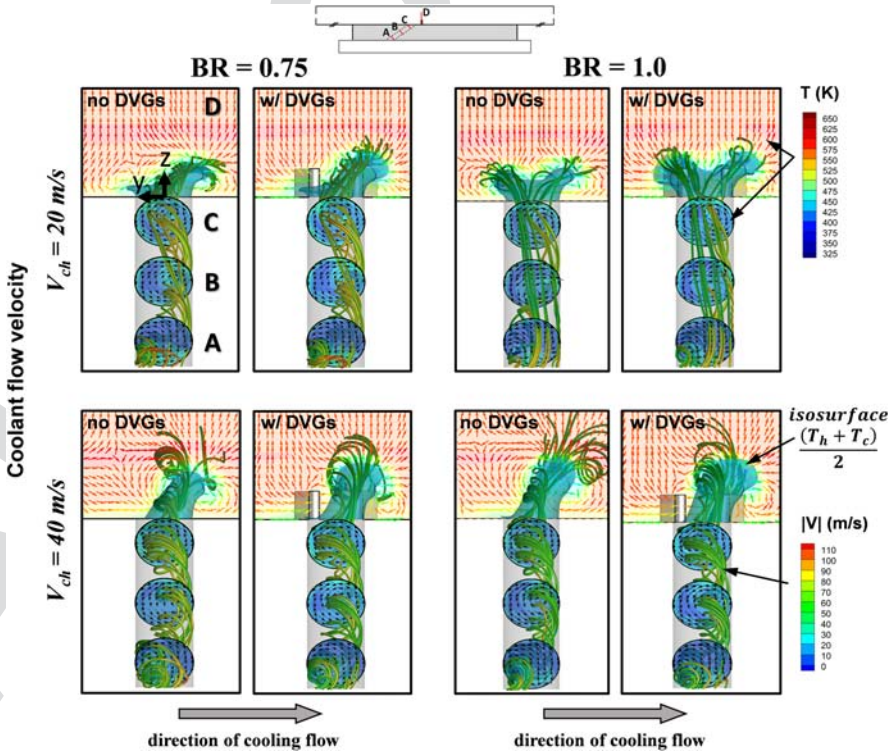

Fig. 11 Velocity vectors in A, B, and C planes and velocity vectors in D colored by temperature (streamlines colored by velocity magnitude)

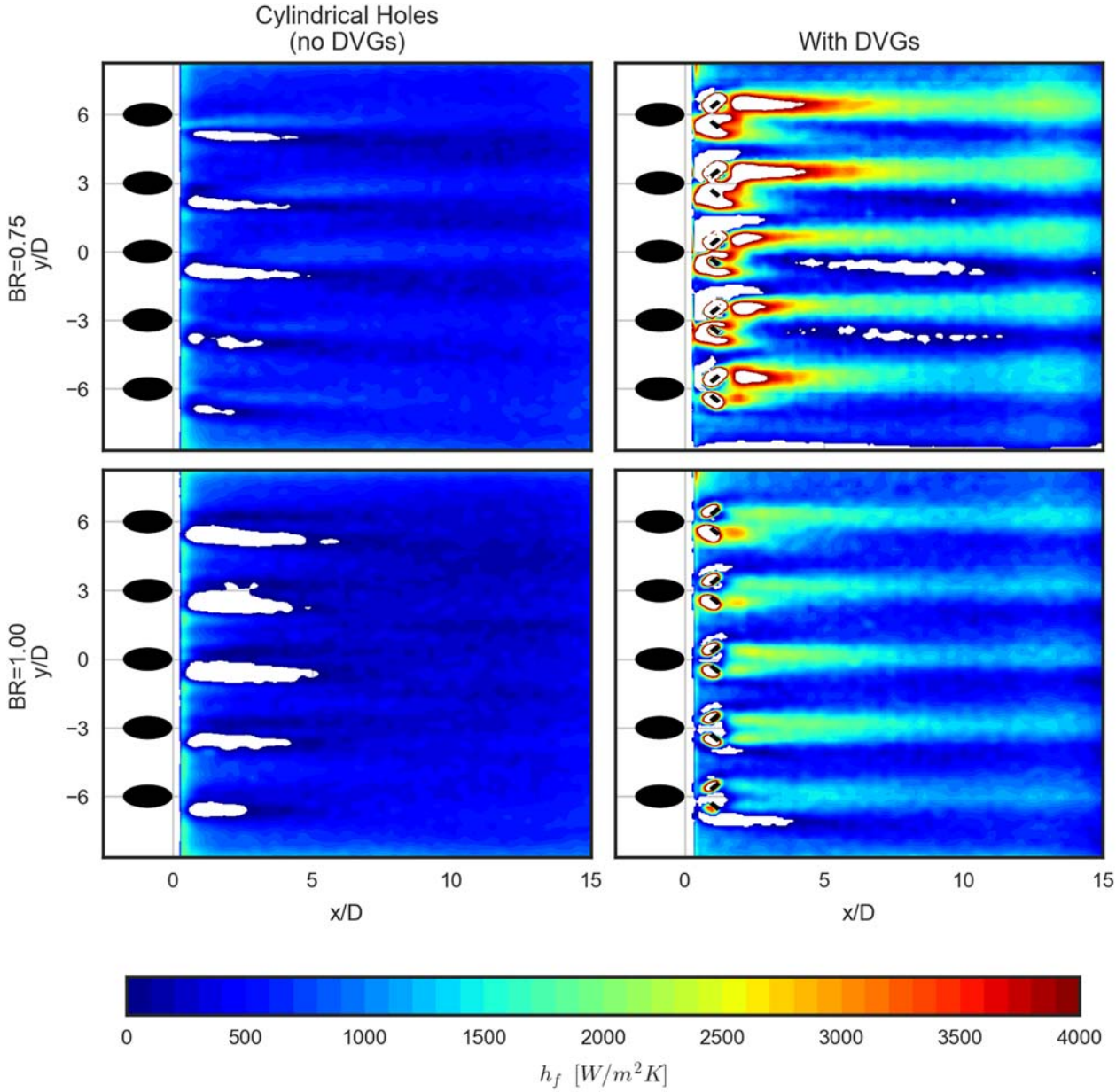

Fig. 13 Local heat transfer coefficient contours (mean-square error is 10–15% based on regression analysis)

consistent with both the CFD and experiment, but the differences are much larger in the experiments. The differences between the experiment and the model are most likely due to boundary conditions. The air gaps surrounding the film-cooling holes (see Fig. 6) are not included in the CFD model, and the walls of the test section are not adiabatic in the experiment.

In theory, the cooling effectiveness curve should have a smooth exponential relationship with coolant mass flowrate, the significant change in slope that is observed in Fig. 12(*b*) (BR = 1.0 with DVGs) may be indicative of jet "lift-off," but more data are needed to confirm that "lift-off" is responsible for the inflection observed in these cooling technology curves.

Since the experimental approach is predicated on the assumption that the film temperature does not change significantly as the coolant channel velocity is varied, the subsequent discussion of experimental results will be restricted to the data points in the blue-shaded regions in Fig. 12. In other words, the data set will be restricted to three inlet velocity ratios and two blowing ratios for each film-cooling design. The lowest inlet velocity ratio is not replicated, so five data points will be included in the linear regression analyses.

Local Heat Transfer Coefficient Contours. The experimental local heat transfer coefficients are shown in Fig. 13. The area of interest shown in Fig. 13 includes all five cooling holes. The white regions within the region of interest (ROI) represent regions where the slope from the regression was less than zero. These regions are ignored in the subsequent film effectiveness contours and laterally averaged results. The DVGs exhibit significantly higher local heat transfer coefficients relative to the cylindrical holes without DVGs. At the lower blowing ratio, the heat transfer enhancement is biased toward the upstream (windward) side of the hole with respect to the cooling flow direction. The results in Fig. 13 also show that the heat transfer enhancement decays between the first hole (most upstream with respect to the coolant flow) to the last hole in the row. To the authors' knowledge, this enhancement in heat transfer has not been presented previously

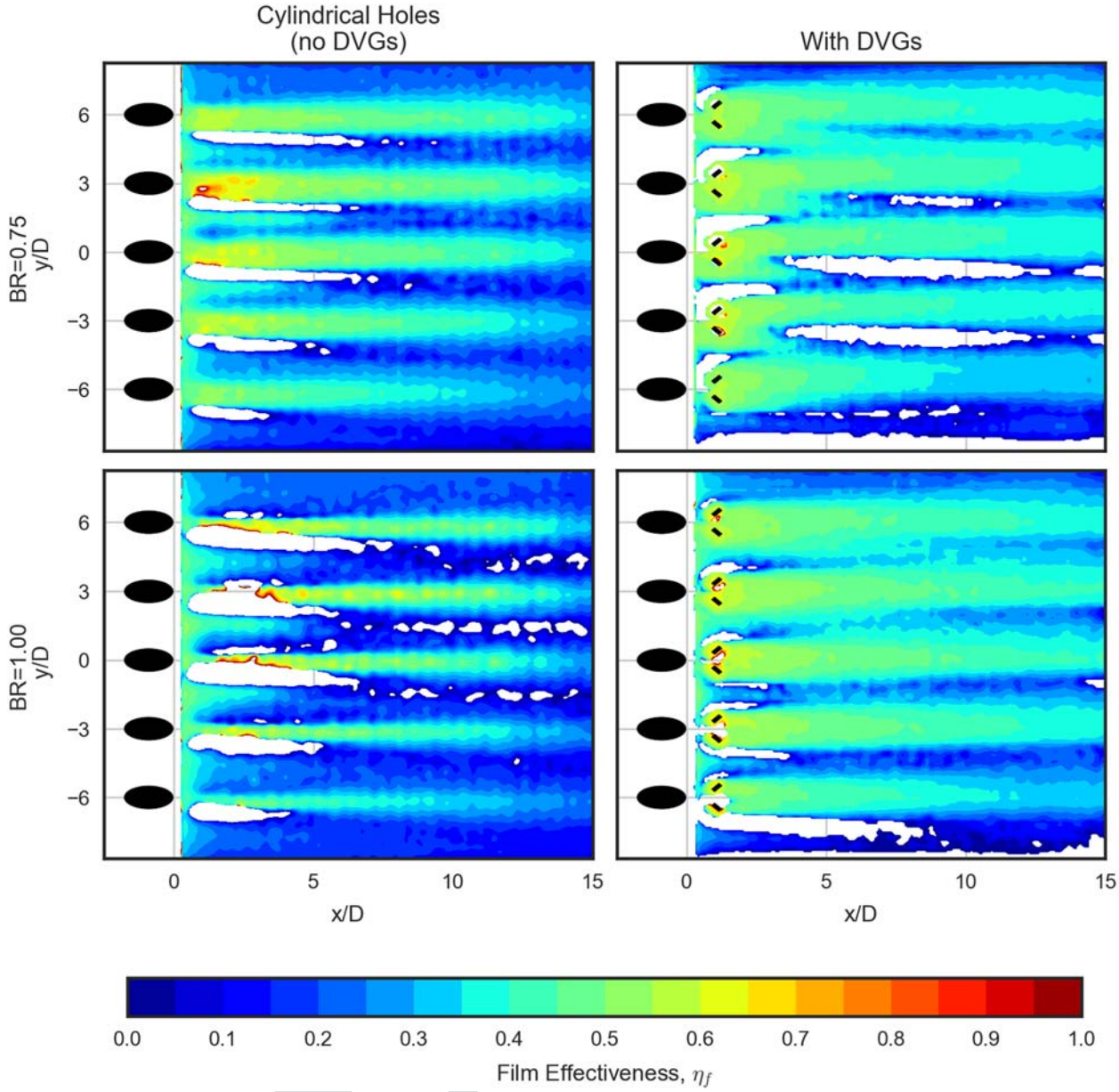

Fig. 14 Experimental local film effectiveness contours (mean-square error is 20–30% based on regression analysis)

for "V-shaped" DVGs in a perpendicular coolant crossflow configuration.

Local Film Effectiveness Contours. The local film effectiveness measurements for BR = 0.75 and BR = 1.0 are shown in Fig. 14. The white regions in this plot represent regions where the regression coefficients are not physically realistic, so these regions are ignored in subsequent analyses. The DVGs produce more jet spreading and coverage than the cylindrical film holes without DVGs, particularly for BR = 1. When comparing the effect of the blowing ratio, the lower blowing ratio (BR = 0.75) generates better film effectiveness for the cylindrical holes without DVGs. The opposite BR effect is observed for the DVGs. Based on the CFD results from Fig. 11, the crossflow effects are more pronounced at the lower blowing ratio, so the cylindrical holes perform better, and the DVGs are less effective.

The local film effectiveness contours predicted by the CFD with adiabatic walls are shown in Fig. 15. The enhanced jet spreading and film coverage are predicted by the CFD, but the local film effectiveness values differ significantly from the experimental values. Some plausible explanations include differences in the boundary conditions (i.e., adiabatic versus conjugate), and the experimental uncertainties in the film effectiveness are significant (i.e., 20–30%).

Laterally Averaged Heat Transfer Coefficients. The laterally averaged heat transfer coefficients for both blowing ratio conditions and both film-cooling designs are shown in Fig. 16. For the DVGs, film effectiveness values are not shown between the cooling hole and the DVGs (i.e., $x/D < 1.5$). For $x/D > 1.5$, the local heat transfer coefficient is approximately two times higher for the DVGs compared to the cylindrical hole baseline. This level of heat transfer augmentation from the DVGs has not been reported previously.

Laterally Averaged Film Effectiveness. In Fig. 17, the laterally averaged experimental (Fig. 17, left) and CFD film effectiveness results (Fig 17, right) are shown for two different blowing ratio conditions. In all cases, the experimental film effectiveness results fall

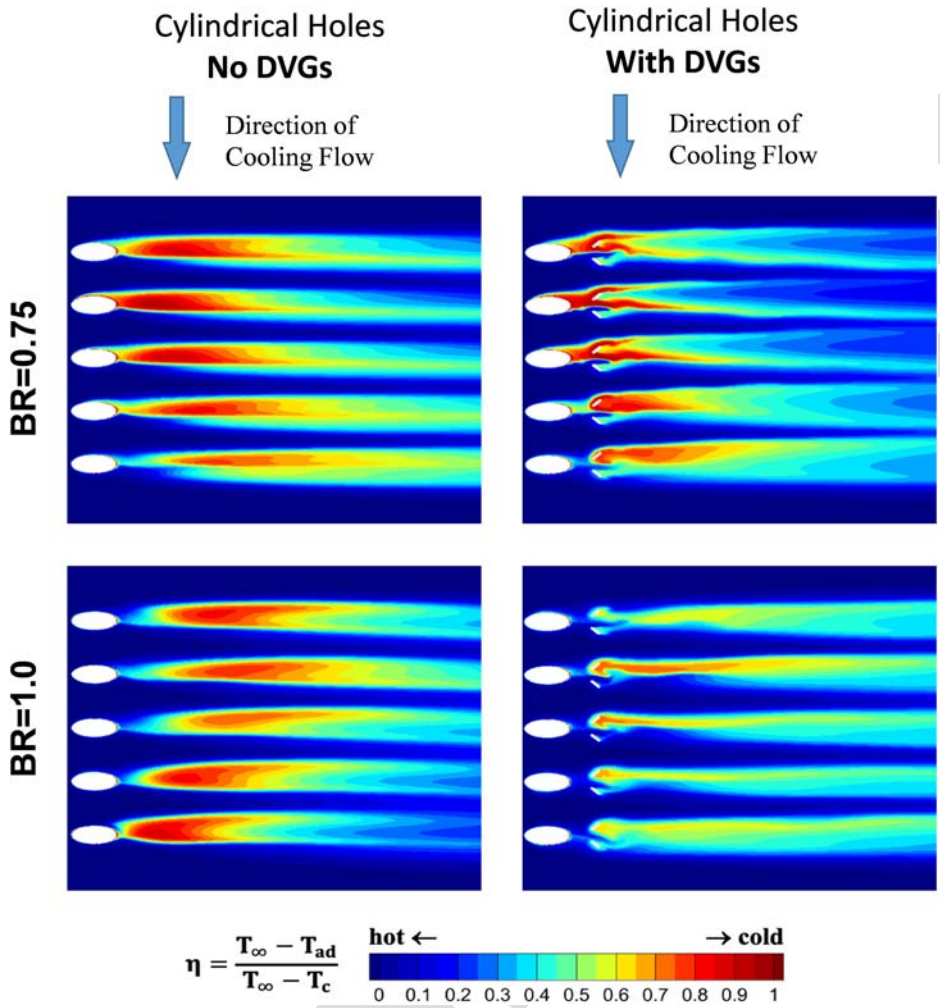

Fig. 15 CFD predictions of local film effectiveness (BR = 0.75→VR_i = 0.52; for BR = 1.0→VR_i = 0.38)

between the CFD predictions for the perpendicular coolant crossflow and the plenum predictions of Lee et al. [30]. For BR = 0.75, the experimental data fall closer to the CFD predictions for perpendicular crossflow. For BR = 1.0, the experimental data fall closer to the CFD predictions for plenum flow. This result is consistent with the CFD results from Fig. 11, which show the flow through the cooling hole is more uniform for BR = 1.0 and low channel cooling velocities (i.e., more like a plenum flow).

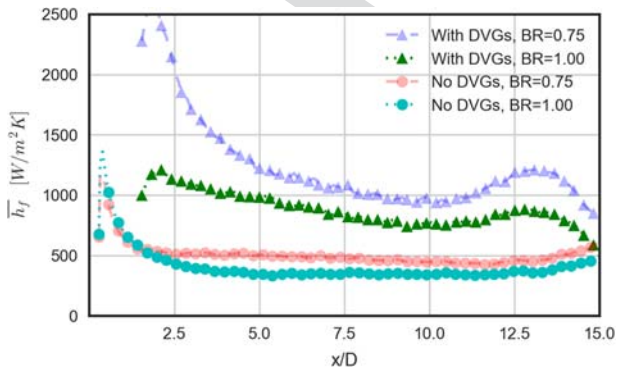

Fig. 16 Laterally averaged heat transfer coefficients—experimental (+ 10–15%)

For BR = 1.0, Fig. 17 shows a relative improvement of about 1.5 times for the DVG design relative to the cylindrical holes without DVGs. This is comparable to the improvement reported by Wang et al. [45] for a different DVG design. However, the present work also shows a much smaller impact for BR = 0.75. In fact, at BR = 0.75, the measured film effectiveness profiles are nearly the same. The CFD results are also very similar for BR = 0.75 with crossflow.

In summary, although the DVGs show a dramatic increase in film effectiveness for a quiescent plenum coolant supply, this benefit can be diminished in a perpendicular coolant crossflow configuration, depending on the blowing ratio and coolant channel velocity. The current work shows the perpendicular coolant crossflow configuration is a significant departure from prior work on "V-shaped" DVGs.

Comparison to Prior Work. In Fig. 18, the laterally averaged film effectiveness measurements are compared to other reported studies on the baseline (i.e., no DVGs) cylindrical hole film-cooling configuration. The work of Baldauf et al. [54] and Sinha et al. [55] utilized a plenum supply without perpendicular crossflow effects. The prior work of Gritsch et al. [41] included perpendicular coolant crossflow effects at coolant channel Mach numbers of 0, 0.3, and 0.6. Only the data for coolant channel Mach numbers of 0 (i.e., plenum) and 0.3 are shown for the cylindrical hole comparison. The channel Mach numbers evaluated in this paper are significantly less than 0.1. Another potential difference between Gritsch

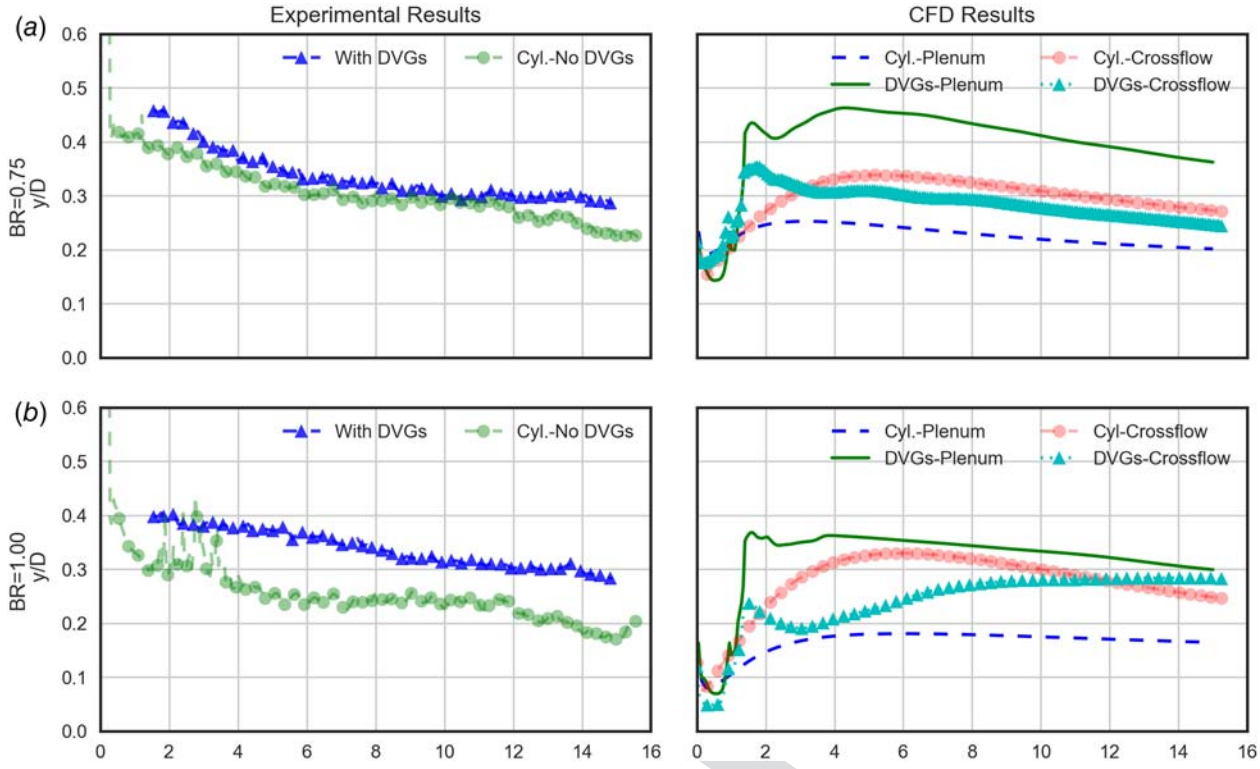

Fig. 17 Laterally averaged film effectiveness: (*a*) BR = 0.75 and (*b*) BR = 1.0

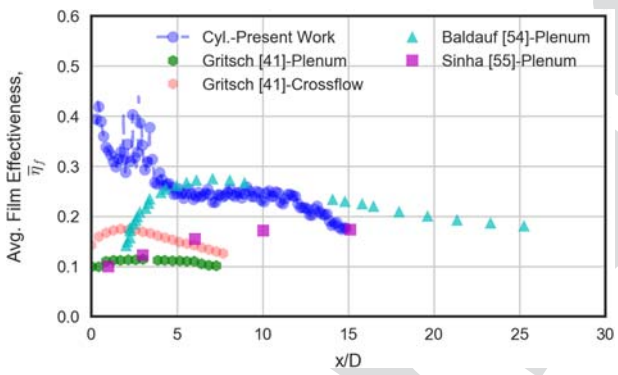

Fig. 18 Comparison of laterally averaged film effectiveness for cylindrical holes (no DVGs) at BR = 1.0 to prior experimental efforts

et al. [41] and the current paper is the direction of the swirl that is imposed on the coolant flow through the hole. In this paper, the direction of the crossflow imposes a counter-clockwise swirl, whereas in Gritsch et al. [41], the coolant jet had a clockwise swirl. It is not clear whether the swirl direction would have a significant effect on the film's effectiveness. Finally, the laterally averaged data presented in this work represent the average over five film-cooling holes, whereas prior crossflow studies have investigated a single film-cooling hole.

Summary and Conclusions

In this paper, numerical and experimental results are presented to evaluate a "V-shaped" downstream vortex generator design described by Lee et al. [9,30] under conditions of perpendicular coolant crossflow. For the experimental study, the hot gas temperature is 650 K, the average Mach number in the freestream is 0.2, the hot-gas-to-coolant temperature ratio is 1.9, and two blowing ratios (0.75 and 1.0) are reported. Local heat transfer coefficients, film effectiveness, and overall cooling effectiveness are measured for a stainless steel (k_w~17 W/m-K) flat plate test article. The conclusions include the following:

- A perpendicular crossflow configuration improves the film effectiveness for cylindrical holes (no DVGs) relative to a plenum-fed configuration (Fig. 17). Thus, there is a potential to reduce the cooling flow and still maintain the same cooling effectiveness with cylindrical holes.
- DVGs can improve effectiveness at BR = 1.0 and low crossflow velocities. However, for higher crossflow velocities, or for lower blowing ratio conditions, the DVGs do not improve cooling effectiveness (Fig. 12).
- The perpendicular coolant crossflow configuration is a significant departure from prior work on "V-shaped" DVGs for a plenum configuration. The amount of swirl in the film-cooling hole depends on the coolant channel velocity and the film-cooling blowing ratio (Fig. 11). Lower cooling channel velocities and higher blowing ratios are less susceptible to swirl effects from the crossflow cooling configurations.
- Although the laterally averaged film effectiveness profiles for the DVG configuration are greater than 0.3 (Fig. 17), the DVGs produce heat transfer coefficients that can be two times larger than cylindrical holes in a perpendicular crossflow configuration (Fig. 16).
- The experimental approach outlined in this paper allows the measurement of heat transfer coefficients, film effectiveness, and overall cooling effectiveness in a single test campaign. This experimental approach is predicated on independent control of the cold-side convective heat transfer coefficient while maintaining constant film-cooling parameters (i.e., blowing ratio, temperature ratio, etc.). The results from this paper show that film-cooling parameters are not always independent of the coolant channel velocity, particularly at high inlet velocity ratios (i.e., VRi > 0.5). In this paper, the experimental technique has been restricted to the lowest coolant

channel velocities (i.e., VRi < 0.5), where the smallest interactions between the film-cooling performance and the crossflow velocity are predicted based on CFD simulations.

Acknowledgment

The authors would like to acknowledge the efforts of Dr. Sridharan Ramesh. His efforts to develop the experimental method were essential to this effort. The authors are grateful to Rich Dennis, Richard Dalton, and Mark Bryden for this support and guidance on the research program. The authors are also grateful for the helpful discussions with Jim Black, Matthew Searle, and Joseph Yip of DOE NETL. This project was funded by the United States Department of Energy, National Energy Technology Laboratory, in part, through a site support contract. Neither the United States Government nor any agency thereof, nor any of their employees, nor the support contractor, nor any of their employees, makes any warranty, express or implied, or assumes any legal liability or responsibility for the accuracy, completeness, or usefulness of any information, apparatus, product, or process disclosed, or represents that its use would not infringe privately owned rights. Reference herein to any specific commercial product, process, or service by trade name, trademark, manufacturer, or otherwise does not necessarily constitute or imply its endorsement, recommendation, or favoring by the United States Government or any agency thereof. The views and opinions of authors expressed herein do not necessarily state or reflect those of the United States Government or any agency thereof.

Funding Data

- The research at Purdue University was supported by the U.S. Department of Energy-Office of Fossil Energy, Advanced Turbines Program under contract No. DE-AC02-07CH11358 through the Ames Laboratory agreement no. 26110-AMES-CMI.

Conflict of Interest

There are no conflicts of interest.

Data Availability Statement

The datasets generated and supporting the findings of this article are obtainable from the corresponding author upon reasonable request.

Nomenclature

h = convective heat transfer coefficient
k = thermal conductivity
p = pitch of cooling hole array
D = film hole diameter
L = length
R = thermal resistance
T = temperature
V = velocity magnitude
k^+ = roughness parameter, $\rho_w u_\tau k_s/\mu_w$
q'' = heat flux
k_s = equivalent sand grain roughness
u_τ = shear velocity
BR = blowing ratio, $\rho_c V_j/\rho_g V_g$
CRV = counter-rotating vortex
DR = density ratio, ρ_c/ρ_g
DVG = downstream vortex generator
Ma = Mach number
Ra = centerline average roughness height
ROI = region of interest
TR = temperature ratio, T_g/T_c
VG = vortex generator
VR = velocity ratio (e.g., $VR_i = V_{ch,i}/V_j$)

Greek Symbols

η = film effectiveness (see Eq. (1))
μ = viscosity
ρ = density
ϕ = overall cooling effectiveness (see Eq. (5))

Subscripts

c = coolant
ch = coolant channel
e = exit
ext = external (hot) surface
f = film
g = hot gas freestream
i = inlet
int = internal (cold) surface
J = cooling jet in film-cooling hole
w = wall (solid)

References

[1] Han, J. C., Dutta, S., and Ekkad, S., 2012, *Gas Turbine Heat Transfer and Cooling Technology*, 2nd ed., CRC Press.
[2] Shih, T. I.-P., and Yang, V., 2014, Turbine Aerodynamics, Heat Transfer, Materials, and Mechanics.
[3] Bogard, D. G., and Thole, K. A., 2006, "Gas Turbine Film Cooling," J. Propul. Power, **22**(2), pp. 249–270.
[4] Bunker, R. S., 2017, "Evolution of Turbine Cooling," ASME Turbo Expo 2017: Turbomachinery Technical Conference and Exposition, ASME Paper No. GT2017-63025.
[5] Uysal, S. C., 2020, "Analysis of Gas Turbine Cooling Technologies for Higher Natural Gas Combined Cycle Efficiency," AIAA Propulsion and Energy 2020 Forum, American Institute of Aeronautics and Astronautics, Reston, Virginia, pp. 1–17.
[6] Goldstein, R. J. R. J., 1971, "Film Cooling," Adv. Heat. Transfer, **7**, pp. 321–379.
[7] Leylek, J. H. H., and Zerkle, R. D. D., 1994, "Discrete-Jet Film Cooling: A Comparison of Computational Results With Experiments," ASME J. Turbomach., **116**(July), pp. 358–368.
[8] Fric, T. F., and Roshko, A., 1994, "Vortical Structure in the Wake of a Transverse Jet," J. Fluid Mech., **279**, pp. 1–47.
[9] Lee, C.-S., Bryden, K., and Shih, T. I. P., 2020, "Downstream Vortex Generators to Enhance Film-Cooling Effectiveness," ASME Turbo Expo 2020: Turbomachinery Technical Conference and Exposition, ASME Paper No. GT2020-14317.
[10] Bunker, R. S., 2005, "A Review of Shaped Hole Turbine Film-Cooling Technology," ASME J. Heat Transfer, **127**(4), pp. 441–453.
[11] Goldstein, R. J., Eckert, E. R. G., and Burggraf, F., 1974, "Effects of Hole Geometry and Density on Three-Dimensional Film Cooling," Int. J. Heat Mass Transfer, **17**(5), pp. 595–607.
[12] Gritsch, M., Colban, W., Schär, H., Döbbeling, K., Schär, H., and Döbbeling, K., 2005, "Effect of Hole Geometry on the Thermal Performance of Fan-Shaped Film Cooling Holes," ASME J. Turbomach., **127**(4), pp. 718–725.
[13] Saumweber, C., Schulz, A., and Wittig, S., 2003, "Free-Stream Turbulence Effects on Film Cooling With Shaped Holes," ASME J. Turbomach., **125**(1), pp. 65–73.
[14] Shih, T. I. P., and Na, S., 2007, "Momentum-Preserving Shaped Holes for Film Cooling," ASME Turbo Expo 2007: Power for Land, Sea, and Air, ASME Paper No. GT2007-27600.
[15] Ligrani, P. M., Wigle, J. M., Ciriello, S., and Jackson, S. M., 1994, "Film-Cooling From Holes With Compound Angle Orientations: Part 1—Results Downstream of Two Staggered Rows of Holes With 3d Spanwise Spacing," ASME J. Heat Transfer, **116**(2), pp. 341–352.
[16] Ligrani, P. M., Wigle, J. M., and Jackson, S. W., 1994, "Film-Cooling From Holes With Compound Angle Orientations: Part 2—Results Downstream of a Single Row of Holes With 6d Spanwise Spacing," ASME J. Heat Transfer, **116**(2), pp. 353–362.
[17] Dittmar, J., Schulz, A., and Wittig, S., 2003, "Assessment of Various Film-Cooling Configurations Including Shaped and Compound Angle Holes Based on Large-Scale Experiments," ASME J. Turbomach., **125**(1), pp. 57–64.
[18] Ekkad, S. V., Zapata, D., and Han, J. C., 1997, "Film Effectiveness Over a Flat Surface With Air and CO2 Injection Through Compound Angle Holes Using a Transient Liquid Crystal Image Method," ASME J. Turbomach., **119**(3), pp. 587–593.
[19] Schmidt, D. L., Sen, B., and Bogard, D. G., 1996, "Film Cooling With Compound Angle Holes: Adiabatic Effectiveness," ASME J. Turbomach., **118**(4), pp. 807–813.

[20] Saumweber, C., and Schulz, A., 2012, "Free-Stream Effects on the Cooling Performance of Cylindrical and Fan-Shaped Cooling Holes," ASME J. Turbomach., **134**(6), p. 061007.
[21] Bunker, R. S., 2002, "Film Cooling Effectiveness Due to Discrete Holes Within a Transverse Surface Slot," ASME Turbo Expo 2002: Power for Land, Sea, and Air, ASME Paper No. GT2002-30178.
[22] Na, S., and Shih, T. I. P., 2007, "Increasing Adiabatic Film-Cooling Effectiveness by Using an Upstream Ramp," ASME J. Heat Transfer, **129**(4), pp. 464–471.
[23] Shih, T. I.-P., Lin, Y.-L., Chyu, M. K., and Gogineni, S., 1999, "Computations of Film Cooling From Holes With Struts," ASME 1999 International Gas Turbine and Aeroengine Congress and Exhibition, ASME Paper No. 99-GT-282.
[24] Zaman, K. B. M. Q., and Foss, J. K., 1997, "The Effect of Vortex Generators on a Jet in a Cross-Flow," Phys. Fluids, **9**(1), pp. 106–114.
[25] Nasir, H., Ekkad, S. V., and Acharya, S., 2003, "Flat Surface Film Cooling From Cylindrical Holes With Discrete Tabs," J. Thermophys. Heat Transfer, **17**(3), pp. 304–312.
[26] Heidmann, J. D., and Ekkad, S., 2008, "A Novel Antivortex Turbine Film-Cooling Hole Concept," ASME J. Turbomach., **130**(3), p. 31020.
[27] Rigby, D. L., and Heidmann, J. D., 2008, "Improved Film Cooling Effectiveness by Placing a Vortex Generator Downstream of Each Hole," ASME Turbo Expo 2008: Power for Land, Sea, and Air, ASME Paper No. GT2008-51361.
[28] Zaman, K. B. M. Q., Rigby, D. L., and Heidmann, J. D., 2010, "Inclined Jet in Crossflow Interacting With a Vortex Generator," J. Propul. Power, **26**(5), pp. 947–954.
[29] Song, L., Zhang, C., Song, Y., Li, J., and Feng, Z., 2017, "Experimental Investigations on the Effects of Inclination Angle and Blowing Ratio on the Flat-Plate Film Cooling Enhancement Using the Vortex Generator Downstream," Appl. Therm. Eng., **119**, pp. 573–584.
[30] Lee, C.-S., Shih, T., Straub, D., Weber, J., and Robey, E. H., 2022, "Computational and Experimental Study of Film-Cooling Effectiveness With and Without Downstream Vortex Generators," ASME J. Turbomach., **145**(2), p. 021007. .
[31] Bohn, D., Ren, J., and Kusterer, K., 2003, "Conjugate Heat Transfer Analysis for Film Cooling Configurations With Different Hole Geometries," ASME Turbo Expo 2003, collocated with the 2003 International Joint Power Generation Conference, ASME Paper No. GT2003-38369.
[32] Gomatam Ramachandran, S., and Shih, T. I.-P., 2015, "Biot Number Analogy for Design of Experiments in Turbine Cooling," ASME J. Turbomach., **137**(6), p. 61002.
[33] Thole, K. A., Gritsch, M., Schulz, A., and Wittig, S., 1997, "Effect of a Crossflow at the Entrance to a Film-Cooling Hole," ASME J. Fluids Eng., **119**(3), pp. 533–540.
[34] Kohli, A., and Thole, K. A., 1998, "Entrance Effects on Diffused Film-Cooling Holes," ASME 1998 International Gas Turbine and Aeroengine Congress and Exhibition, ASME Paper No. 98GT-402.
[35] Gritsch, M., Schulz, A., and Wittig, S., 1998, "Heat Transfer Coefficient Measurements of Film Cooling With Expanded Exits," ASME 1998 International Gas Turbine and Aeroengine Congress and Exhibition, ASME Paper No. 98-GT-28.
[36] Gritsch, M., Schulz, A., and Wittig, S., 1998, "Discharge Coefficient Measurements of Film-Cooling Holes With Expanded Exits," ASME J. Turbomach., **120**(3), pp. 557–563.
[37] Gritsch, M., Schulz, A., and Wittig, S., 2000, "Film-Cooling Holes With Expanded Exits: Near-Hole Heat Transfer Coefficients," Int. J. Heat Fluid Flow, **21**(2), pp. 146–155.
[38] McClintic, J. W., Fox, D. W., Jones, F. B., Bogard, D. G., Dyson, T. E., and Webster, Z. D., 2019, "Flow Physics of Diffused-Exit Film Cooling Holes Fed by Internal Crossflow," ASME J. Turbomach., **141**(3), p. 031010.
[39] McClintic, J. W., Anderson, J. B., Bogard, D. G., Dyson, T. E., and Webster, Z. D., 2018, "Effect of Internal Crossflow Velocity on Film Cooling Effectiveness—Part I: Axial Shaped Holes," ASME J. Turbomach., **140**(1), p. 11003.
[40] McClintic, J. W., Anderson, J. B., Bogard, D. G., Dyson, T. E., and Webster, Z. D., 2018, "Effect of Internal Crossflow Velocity on Film Cooling Effectiveness—Part II: Compound Angle Shaped Holes," ASME J. Turbomach., **140**(1), p. 11004.
[41] Gritsch, M., Schulz, A., and Wittig, S., 2003, "Effect of Internal Coolant Crossflow on the Effectiveness of Shaped Film-Cooling Holes," ASME J. Turbomach., **125**(3), pp. 547–554.
[42] Stratton, Z. T., 2014, "Effects of Crossflow in an Internal-Cooling Channel on Film Cooling of a Flat Plate Through Compound-Angle Holes," Purdue School of Mechanical Engineering. Q17
[43] Qenawy, M., Zhou, W., and Liu, Y., 2022, "Effects of Crossflow-Fed-Shaped Holes on the Adiabatic Film Cooling Effectiveness," Int. J. Therm. Sci., **177**(Feb.), p. 107578.
[44] Sperling, S. J., and Mathison, R. M., 2022, "Time-Accurate Evaluation of Film Cooling Jet Characteristics for Plenum and Crossflow Coolant Supplies," J. Therm. Sci. Eng. Appl., **14**(4), pp. 1–12.
[45] Wang, J., Zhang, C., Liu, X., Song, L., and Li, J., 2022, "Experimental and Numerical Investigation on the Film Cooling Performance of Cylindrical Hole and Fan-Shaped Hole With Vortex Generator Fed by Crossflow," Int. J. Heat Mass Transfer, **187**, p. 122560.
[46] Menter, F. R., Kuntz, M., and Langtry, R., 2003, "Ten Years of Industrial Experience With the SST Turbulence Model," 4th International Symposium on Turbulence, Heat and Mass Transfer, pp. 625–632.
[47] Kim, C. S., 1975, "Thermophysical Properties of Stainless Steels," Argonne, IL.
[48] "ANSYS FLUENT Computational Fluid Dynamic Code, Release 17.1."
[49] Kneer, J., Puetz, F., Schulz, A., and Bauer, H.-J., 2016, "A New Test Facility to Investigate Film Cooling on a Nonaxisymmetric Contoured Turbine Endwall—Part II: Heat Transfer and Film Cooling Measurements," ASME J. Turbomach., **138**(7), p. 71004.
[50] Ramesh, S., Robey, E. H., Lawson, S., Straub, D. L., and Black, J. B., 2020, "Design Flow Field, and Heat Transfer Characterization of Conjugate Aero-Thermal Test Facility at NETL," ASME Turbo Expo 2020: Turbomachinery Technical Conference and Exposition, ASME Paper No. GT2020-15644.
[51] Bons, J. P., 2010, "A Review of Surface Roughness Effects in Gas Turbines," ASME J. Turbomach., **132**(2), p. 021004.
[52] Searle, M., Roy, A., Black, J., Straub, D., and Ramesh, S., 2022, "Investigating Gas Turbine Internal Cooling Using Supercritical CO_2 at Higher Reynolds Numbers for Direct Fired Cycle Applications," ASME J. Turbomach., **144**(1), p. 011007.
[53] Schaffler, A., 1980, "Experimental and Analytical Investigation of the Effects of Reynolds Number and Blade Surface Roughness on Multistage Axial Flow Compressors," J. Eng. Power, **102**(1), pp. 5–12.
[54] Baldauf, S., Scheurlen, M., Schulz, A., and Wittig, S., 2002, "Correlation of Film-Cooling Effectiveness From Thermographic Measurements at Enginelike Conditions," ASME J. Turbomach., **124**(4), pp. 686–698.
[55] Sinha, A. K. K., Bogard, D. G., and Crawford, M. E., 1991, "Film-Cooling Effectiveness Downstream of a Single Row of Holes With Variable Density Ratio," ASME J. Turbomach., **113**(3), pp. 442–449.